

Large Eddy Simulation on Development and Evolution of Subsonic-Supersonic Shear Mixing Layer

Liu Yang, Fu Ben-shuai and Zhang Chen-xi
Corresponding author: liuyang802@nwpu.edu.cn

Science and Technology on Combustion, Internal Flow and Thermo-structure
Laboratory, Northwestern Polytechnical University, Xi'an, China, 710072.

Abstract: Subsonic-supersonic shear mixing flow is one of important research field in turbulence research. In the rocket ramjet combustion chamber, the mixing of main rocket gas and air is a typical large gradient subsonic-supersonic shear mixing flow, which has characteristics of high convective Mach number (Mc) and large flow parameter gradient. It is of great significance to study the development rule and flow structure of the large gradient subsonic-supersonic shear mixing flow, which is of great significance to enhance the blending and enhance the working performance of the ramjet engine. High temperature and high speed subsonic-supersonic shear mixing flow experimental measurement is quite difficult, and it can receive far less information than incompressible shear mixing flow and compressible shear mixing flow of normal temperature state. In this paper, the high order precision numerical simulation of high temperature and high speed shear mixing flow is carried out by means of large eddy simulation (LES). A total of 6 groups of simulation are carried out, the Mc ranges from 0.87 to 1.67, total temperature of primary stream ranges from 1000K to 1800K, the main flow characteristics and the growth rate rule of shear mixing layer thickness under the condition of different inflow parameters are obtained. Analyzing the growth rate of shear mixing layer thickness under the condition of different inflow parameters, the following rules are founded: In the aspect of statistical parameter such as thickness growth rate, turbulence intensity and Reynolds stress, the rules of shear mixing flow with strong compressibility and weaker compressibility are similar; When compressibility increases from medium to high, the growth rate of shear mixing layer falls dramatically, and as compressibility continues to increase, with Mc reach 1.44 above, the growth rate of shear mixing layer slightly decreases, and the growth rate is small enough at this time; In large gradient shear mixing flow, it is difficult to form large scale coherent structure in the supersonic region due to the influence of primary stream compressibility; Analyzing two kinds of characterization parameters of Mc and Π_c , the characterization effect of Π_c is better than that of Mc on high compressibility shear mixing flow.

Keywords: Subsonic-supersonic shear mixing flow, Large Eddy Simulation, Convective Mach Number (Mc), Π_c .

1 Introduction

In rocket ramjet combustion chamber, shear mixing layer of two jet streams grows quite slowly along with the flow. And in the limited length of the combustion chamber, energy and momentum transfer between two jet streams can't finish effectively, which caused the overall combustion efficiency of the main ramjet combustion chamber low and the fuel energy not give full play to, even serious impact on the performance of combined engine. So it becomes one of technology bottlenecks of combined engine research.

For the understanding of turbulent mixing, the first is the study of incompressible mixing flow at low speed. Under the background of hypersonic flight vehicle research, shear mixing layer research expands gradually to compressible mixing flow. Previous studies show that the growth rate of shear mixing layer, turbulence intensity and Reynolds stress decrease due to compressibility of flow, and the stability of shear mixing layer increases. When compressibility is further strengthened, it is difficult to form large scale coherent structure.

Bogdanoff [1] et al. proposed the concept of convective Mach number (Mc) for the first time, which is a dimensionless parameter that characterizes the development of large scale coherent structure of shear mixing layer. Papamoschou [2, 3] further refined the definition of Mc , and found that the growth rate of shear mixing layer obtained in the experiment could be used to fit a curve.

A lot of experimental researches show that, compared with incompressible shear mixing layer [4], the compressibility of compressible shear mixing layer in the static pressure, temperature and density ratio and other conditions remain unchanged, have larger inhibition to the growth rate of shear mixing layer. Summarizing the experimental data, we can find the dimensionless growth rate of most of experiment research obtained (under the condition of same density ratio and velocity ratio, as the growth rate of incompressible shear mixing layer dimensionless parameters) and Mc have a better fitting relationship, while $Mc < 0.6$, as shown in figure 1.

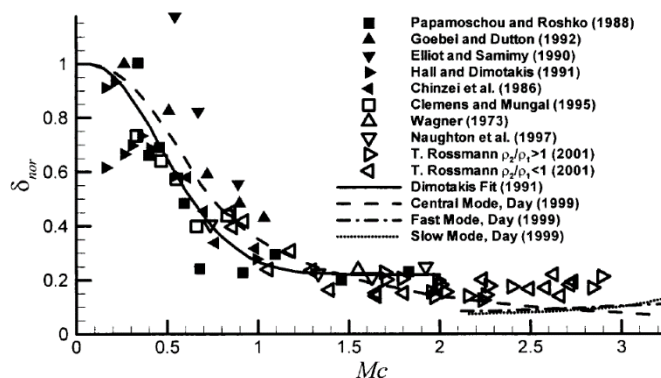


Figure 1: Comparison of the results of previous studies on the growth rate of compressible shear mixing layer [2, 5-13].

However, when the density ratio and the velocity ratio of shear mixing layer deviate from one, the growth rate of experiment obtained is very different from that of fitting curve. Slessor [14] et al. believe that this is due to the limitation of independent variable Mc . The premise of Mc is isentropic assumption, while the shear mixing layer often no longer meet isentropic hypothesis at this time, so they put forward a new parameter, Πc . In larger scope of Πc , they obtained fitting curve of the dimensionless parameter with experimental data, as shown in figure 2.

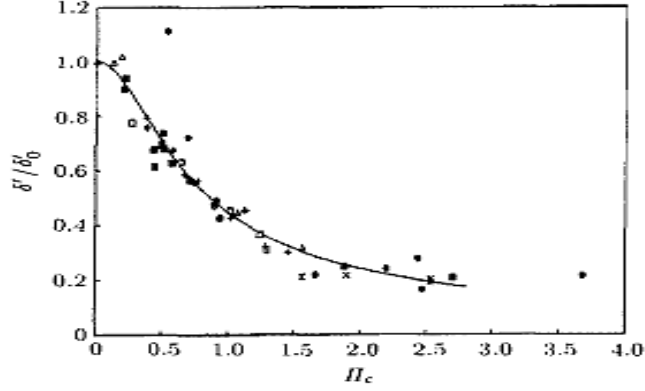


Figure 2: Relationship between the dimensionless growth rate of the shear mixing layer and Π_c [15].

Relationship between the growth rate of shear mixing layer with quantitative characterization parameters, its significance is not only a summary of a large number of experimental data, but also to determine the algebraic relationship between the growth rate of shear mixing layer with quantitative characterization parameters. On the one hand, it can be used to simple estimate the growth rate of shear mixing layer, which is hard to get through the experiment, as well as the establishment of theoretical model and the engineering application. On the other hand, it is also an evaluation standard of follow-up experiment and numerical simulation study⁵.

With the development of computer technology, computational fluid dynamics (CFD) method has made great progress and development, and it has become one of the main approaches to turbulence study, and a beneficial supplement of the theoretical and experimental research. Numerical simulation plays an important role in the study of the three-dimensional flow structure of shear mixing layer and the instability of K-H et al. In turbulence study, the commonly used CFD technology is Direct Numerical Simulation (DNS) [16], Large Eddy Simulation (LES) [17] and Reynolds Averaged Numerical Simulation (RANS) et al.

LES is different from RANS and DNS. This method is based on transport and dissipation of turbulent pulsations at different flow scales. The large scale turbulence pulsation in the flow contains the main momentum and energy, which dominates momentum and energy transport of turbulent pulsation; however, small scale flow structure contains less energy, which mainly plays a role of dissipative. The basic idea of LES is decomposing flow scale into large scale and sub-grid scale through a low-pass filter, solving large scale flow directly, and simulating the effect of small scale flow to large scale flow through turbulence model. Compared with DNS, the accuracy of LES decreases, but computation amount required is much less. Compared with RANS, main advantages of LES lie in that it only needs model to characterize the sub-grid flow scale, and calculation results is more accurate relatively. Therefore, LES provides a way to solve complex turbulence at this stage of computing power.

The LES application early was also carried out in the incompressible flow. Doris [18] et al. used the LES method to study the three-dimensional compressible shear flow, and the convection Mach number was 0.64, the number of mesh is $512 \times 59 \times 59$, and Re is 60000 based on the inlet momentum thickness. The results show that both flow direction and transverse pulsation velocity have self-similar behavior, but the LES method is too high to estimate the velocity pulsation in the core area of the shear mixing layer. These results show that LES is effective in calculating the complex flow of weak compressibility.

At present, there is a lot of research on shear mixing flow at home and abroad, and great progress has been made, but there are still many shortcomings.

2 LES simulation

2.1 LES model

The basic control equations for describing turbulence process are compressible Navier-Stokes equations. The LES turbulence control equations can be obtained through Favre average and then filtering of the continuity equation, momentum equation, energy equation and composition equation. The LES method thinks flow parameter f is composed of two parts of linear superposition, can be expressed as $f = \tilde{f} + f''$, where \tilde{f} represents the large eddy scale could be solved directly, and f'' represents the sub-grid scale. The flow parameters can be expressed as $\tilde{f} = \overline{\rho f} / \bar{\rho}$ after Favre average (mass-weighted average), where \tilde{f} represents spatial filtering, defined as:

$$\overline{\rho f(x_i, t)} = \int_D \rho f(z_D, t) g(x_i - z_i, \Delta) dz_i$$

Where g is the filter function; D is the integral region; Δ is the filter scale, defined as $\Delta = (\Delta x \Delta y \Delta z)^{1/3}$ in this paper, and where Δx , Δy and Δz represent the three-dimensional space grid scale respectively.

The simple filtering function adopted in this paper is:

$$g = \begin{cases} 1/\Delta & -\Delta/2 \leq (x - z) \leq \Delta/2 \\ 0 & \text{otherwise} \end{cases}$$

The spatial filtering equation is applied to the above two equations, then we can get LES control equations, as shown in the following three equations:

$$\begin{aligned} \frac{\partial \bar{\rho}}{\partial t} + \frac{\partial}{\partial x_i} (\bar{\rho} \tilde{u}_i) &= 0 \\ \frac{\partial}{\partial t} (\bar{\rho} \tilde{u}_i) + \frac{\partial}{\partial x_j} (\bar{\rho} \tilde{u}_i \tilde{u}_j) &= \frac{\partial}{\partial x_j} (-\delta_{ij} \bar{P} + \tilde{\tau}_{ij} - \tau^{sgs}) \\ \frac{\partial}{\partial t} (\bar{\rho} \tilde{h}) + \frac{\partial}{\partial x_j} (\bar{\rho} \tilde{h} \tilde{u}_j + h_j^{sgs} + \bar{p} u_j) &= \frac{\partial}{\partial x_j} (\tilde{q}_j + \tilde{\tau}_{ij} \tilde{u}_i + \sigma_j^{sgs}) \end{aligned}$$

Where $\tilde{\tau}_{ij} = \mu \left[\left(\frac{\partial \tilde{u}_i}{\partial x_j} + \frac{\partial \tilde{u}_j}{\partial x_i} \right) - \frac{2}{3} \delta_{ij} \frac{\partial \tilde{u}_k}{\partial x_k} \right]$, $\tilde{q}_j = k \frac{\partial \tilde{T}}{\partial x_j}$.

And the sub-grid of new generation can be represented as:

$$\tau^{sgs} = -2\nu_{ij} \tilde{S}_{ij} + \frac{1}{3} \delta_{ij} \tau_{kk}$$

In the LES, the sub-grid stress term can't be calculated from the solvable scale directly, so the solution of sub-grid stress needs to be closed by introducing model. The closure of turbulence sub-grid term, namely the simulation of sub-grid viscous coefficient, is usually based on the assumption of turbulence eddy viscosity. The Smagorinsky model proposes the initial simulation method:

$$\nu_t = (C_s \Delta)^2 (2\tilde{S}_{ij} \tilde{S}_{ij})^{1/2}$$

Where C_s is Smagorinsky constant, which needs to be predetermined in numerical simulation.

Fixed C_s can't adapt to the different state of full flow range, so the method of dynamic calculating Smagorinsky constant based on the solvable velocity field is proposed, which is the Dynamic Smagorinsky-Lilly model.

The LES in this paper is closed with Stretched-Vertex Subgrid-Scale Model, which is proposed by Pullin [19]. The model assumes that the flow within the sub-grid scale is caused by the vortex in the sub-grid, and the small scale vorticity is constructed by symmetrical vortex structure. Currently, the model has been successfully used in the estimation of turbulence mixing and sub-grid energy spectrum.

The above equations are closed by the state equation:

$$p = \rho RT$$

Considering the relatively sharp temperature changes in shear flow, the calculation of gas viscosity is based on Sutherland formula:

$$\mu = \mu_0 \frac{T_0 + C}{T + C} \left(\frac{T}{T_0} \right)^{3/2}$$

Where $\mu_0 = 1.827 \times 10^{-5} Pa \cdot s$, $C = 120K$, $T_0 = 291.5K$.

In the published literature at home and abroad, it is difficult to obtain the comprehensive of great gradient subsonic-supersonic shear mixing layer velocity field information, so experimental data of normal temperature subsonic-supersonic shear mixing layer carried out by Goebel [20] is adopted for numerical validation LES model using in this paper. Figure 3 shows the shear mixing layer velocity profile expressed in self-similar form, and it can be found that numerical result is in good agreement with experiment data.

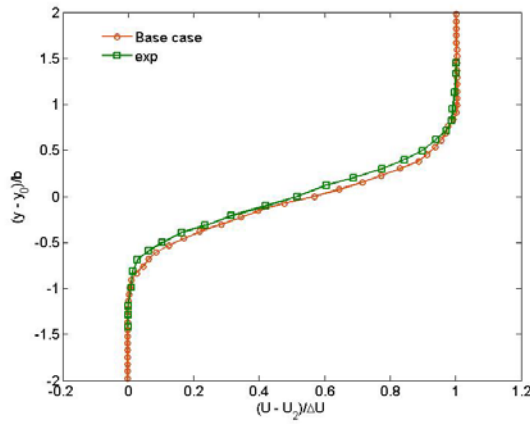


Figure 3: Comparison of shear mixing layer velocity profile between numerical result and experimental data.

2.2 Calculation parameters

In this paper, the classical plane shear flow configuration is adopted, shown in figure 4. In the cube flow region, the upper part is supersonic flow (primary stream), the lower part is subsonic airflow (secondary stream), the left side is entrance, the right side is export, and the top and bottom surface of the wall. In the flow area, the length is 500mm, the height is 60mm, and primary stream and second flow each account for 30mm, and the thickness is 30mm; using uniform grid, the number of each direction is $1250 \times 150 \times 60$.

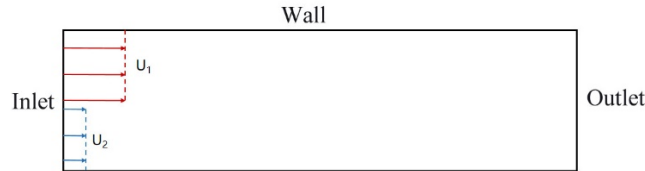


Figure 4: Schematic diagram of flow region.

At high and low velocity inlet, velocity and static temperature are given, and random distribution disturbance is added to the velocity field to simulate the fully developed turbulent inlet and shorten

the computation time. Given static pressure at the high speed inlet, and the low speed inlet pressure is obtained by extrapolation. The exit is zero gradient boundary condition. The partition is non-slip boundary condition, the wall is sliding wall surface, and the front and back wall are periodic boundary conditions.

In this paper, AMROC-VTF is adopted, which is a hydrodynamic solver based on finite volume method. In the numerical calculation, time term is solved by the third-order R-K method, and space term uses the fourth-order WENO-TCD format. CFL condition is used to control time step in the calculation, and the CFL condition number is 0.9.

In this paper, a total of 6 LES were carried out, and the range of Mc was 0.87-1.67, which included the shear flow of moderate compressibility and strong compressibility. The pressure is constant pressure, the change range of the total temperature of primary stream is 1000K-1800K, and the subsonic-supersonic shear flow of high temperature state is mainly studied.

Table 1: Flow parameters table.

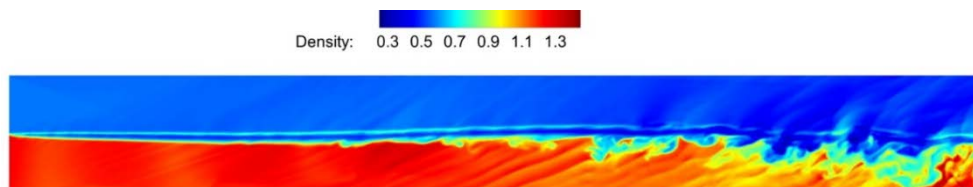
Secondary stream		Primary stream					
		C1	C2	C3	C4	C5	C6
Ma	0.3	3	2.5	2	1.5	2.36	1.58
T, K	294.7	642.9	800.0	1000.0	1241.4	473.1	800.4
T0, K	300	1800	1800	1800	1800	1000	1200
U, m/s	103.2	1524.7	1417.4	1267.6	1059.4	1028.9	896.0
Mc	-	1.67	1.44	1.19	0.91	1.19	0.87

C1, C2, C3 and C4 as a group, keep total temperature of primary stream unchanged, and change Ma of primary stream. In the two groups of C2 and C6, static temperature is same, and Ma is different, so as to analyze the influence of temperature on development of shear mixing layer. The two groups of C3 and C5 have the same number of Ma , but there is a large difference in parameters of primary stream, so as to study the applicability of compressibility of shear mixing layer is characterized by Mc .

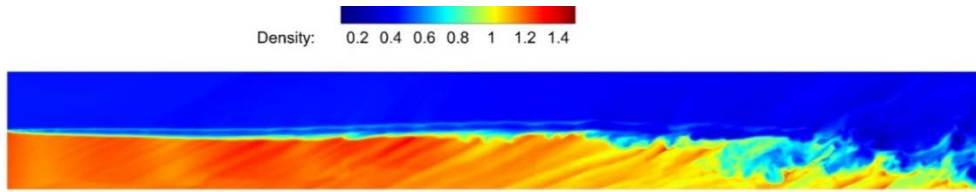
3 Main results

3.1 Density distribution

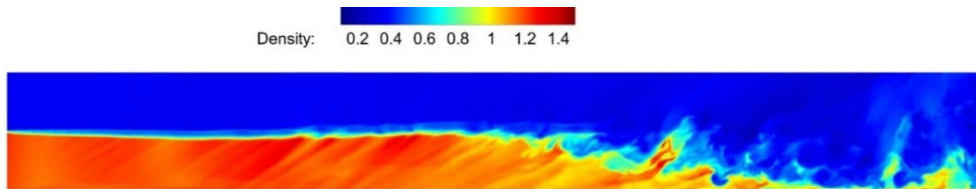
Density field obtained by calculation is displayed, as shown in figure 5, (a) - (f) is the density contour map of each group of C1-C6 along the XY plane.



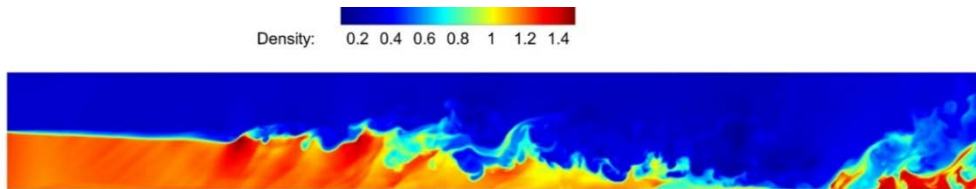
(a) Density contour of C1.



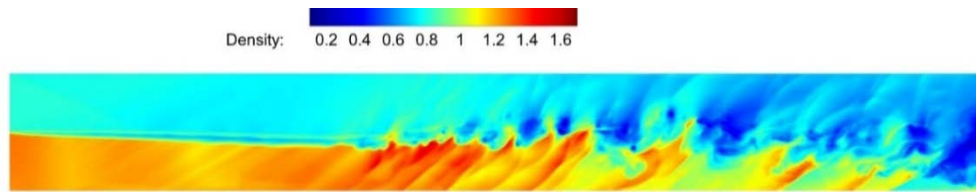
(b)Density contour of C2.



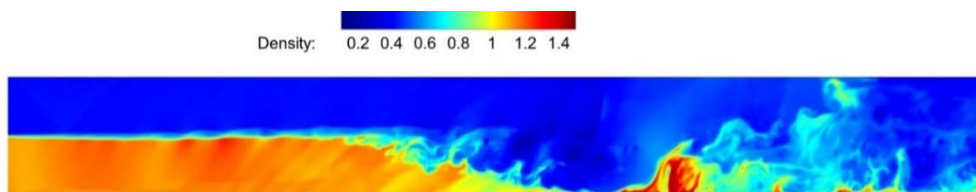
(c)Density contour of C3.



(d)Density contour of C4



(e)Density contour of C5



(f)Density contour of C6

Figure 5: Density contours of C1-C6.

For the gradient of the density field of shear mixing flow, we can obtain the numerical schlieren contour. It is shown that the change of flow structure in the flow field can be observed clearly by using dark color in the region with large variation of density gradient in flow.



(a) Numerical schlieren contour of C1.



(b) Numerical schlieren contour of C2.



(c) Numerical schlieren contour of C3.



(d) Numerical schlieren contour of C4.



(e) Numerical schlieren contour of C5.



(f) Numerical schlieren contour of C6.

Figure 6: Numerical schlieren contours of C1-C6.

Compressibility of C1-C6 six groups is strong, and there is no significant and identifiable large scale coherent structure. The detail difference between strong compressibility shear mixing flow and weak compressibility shear mixing flow lies in identifiability of large scale coherent structures, this point shown well in the numerical simulation of this paper.

C1 is the group with the largest Mc in 6 groups, it keeps laminar state at a long distance after the two streams meet, then transforms to turbulence, and the transition location is not fixed. The vortex structure of shear mixing layer increases gradually of downstream direction and produces a large number of small scale vortex structures.

C6 is the group with the smallest group in the 6 groups, and the most violent one of momentum exchange along the tangential direction.

The Mc of C1-C4 four groups decreased successively. It can be found that the flow transition delay, the mixing region becomes thinner and mainly concentrated in the low speed region with Mc increasing.

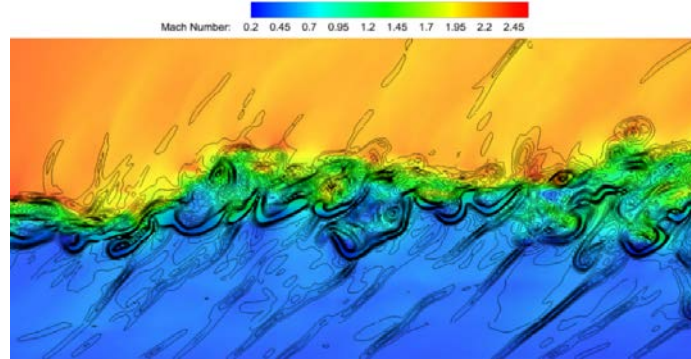


Figure 7: Small shock structure in C5 shown in the way of density gradient contour.

Small shock structure is observed in the high compressible shear mixing flow. Due to the sparse grid, the small shock structure can't be captured well, as shown in figure 7.

3.2 Flow characteristics of shear mixing layer

3.2.1 Shear mixing layer thickness

Small shock structure is observed in the high compressible shear mixing flow. Due to the sparse grid, the small shock structure can't be captured well, as shown in figure 7.

For definition of shear mixing layer thickness, vorticity thickness can be used:

$$\delta_{\omega} = \frac{\Delta U}{\left(\frac{\partial U}{\partial y}\right)_{max}}$$

Or momentum thickness: $\delta = y_{U1-0.1\Delta U} - y_{U2+0.1\Delta U}$. Shear mixing layer thickness is calculated by using the definition of momentum thickness here.

Figure 8 shows the thickness of the shear mixing layer of downstream direction of C1-C6 groups. It can be found that the shear mixing layer thickness varies greatly in the calculated condition ($0.87 \leq Mc \leq 1.67$).

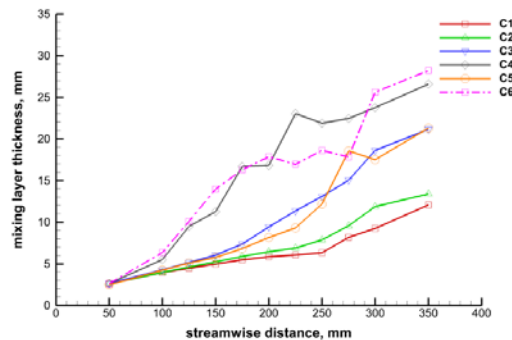


Figure 8: Shear mixing layer thickness of C1-C6.

1) Influence of Mc

C1, C2, C3 and C4 four groups are same in secondary stream parameters and primary stream temperature, while primary stream Ma is different, and their Mc are 1.67, 1.44, 1.19, 1.44 respectively, and the purpose is to analyze the influence of Mc on the growth rate of shear mixing layer thickness.

Figure 9 shows the shear mixing layer thickness of downstream direction of C1-C4 four groups. It can be found that the growth rate of shear mixing layer thickness decreases rapidly when the Mc increases, and the shear mixing layer thickness growth rate of $Mc=0.91$ is roughly 2.5 times that of $Mc=1.67$. When Mc continues to increase from 1.44, the decrease of shear mixing layer growth rate decreases, and all of them maintain a relatively small growth rate.

C1 and C2 two groups are similar, which shows that the influence of compressibility on growth rate decreases, when Mc increases to 1.4.

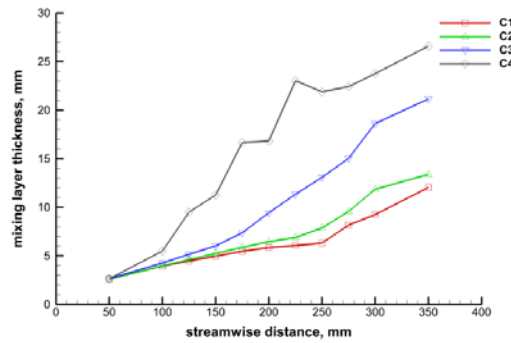


Figure 9: Shear mixing layer thickness of C1-C4.

2) Influence of temperature

C2 and C6 two groups have same primary stream static temperature and different Mc , and the Mc of C2 group is 1.44 and the C6 is 0.87. The two groups have large difference, in order to analyze influence of static temperature on the development of shear mixing layer.

Figure 10 shows the curves of shear mixing layer thickness of downstream direction of C2 and C6. It can be found that the growth rate of C6 is significantly greater than that of C2, indicating that static temperature has less influence on the shear mixing layer thickness growth rate.

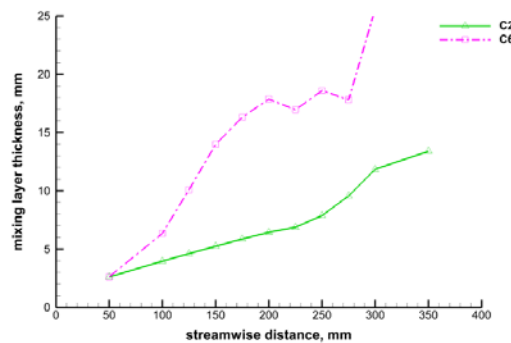


Figure 10: Shear mixing layer thickness of C2 and C6.

From the previous section, in C1-C4 four groups, total temperature of primary stream is same, and shear mixing layer thickness growth rate shows decreases with the Mc increases, and the characteristic is similar to that of a weak compressibility shear mixing flow. It shows that one of affection factor directly of shear mixing flow growth rate is Mc , not total temperature. The total temperature affects the temperature and velocity, and then affects the Mc .

3) Influence of other parameters on the same Mc

The two groups of C3 and C5 have the same Mc , but there is a large difference in the parameters of primary stream, in order to study the applicability of the compressibility of the shear mixing layer is characterized by the Mc .

It can be found from figure 11 that the growth rate of C3 and C5 two groups is approximately same, indicating that other flow parameters have less influence on the growth rate of shear mixing flow.

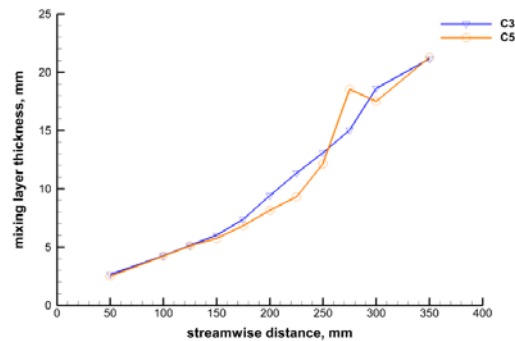


Figure 11: Shear mixing layer thickness of C3 and C5.

3.2.2 Velocity fluctuation

1) $X=100\text{mm}$

Due to the high Mc , no transition of C1, C2, C3 and C5 four groups is started at 100mm of downstream direction, so the turbulence intensity curves of downstream direction of the four groups are similar. At this position, the two groups of C4 and C6 have started to transform, so the turbulence intensity curves of downstream direction of the two groups is "wider" than the first four groups, namely, the range of high turbulence intensity in the string direction is larger. The common characteristic of the six groups is that the peak of the turbulence intensity curves of downstream direction is approximately same.

The performance of turbulence intensity of tangential direction is quite different from that of the turbulent intensity of downstream direction. The two groups of C4 and C6 have undergone transition at 100mm and can see that the peak of turbulence intensity of tangential direction is significantly higher than that of the other four groups without transition. In the case of without transition, the peak value is relatively close, and the parameters such as Mc have less influence. Another difference is that the maximum value of turbulence intensity of tangential direction is obvious shifting to the low velocity region, roughly at $Y=-6\text{mm}$, while the shifting of maximum value of turbulence intensity of downstream direction is no more than 2mm.

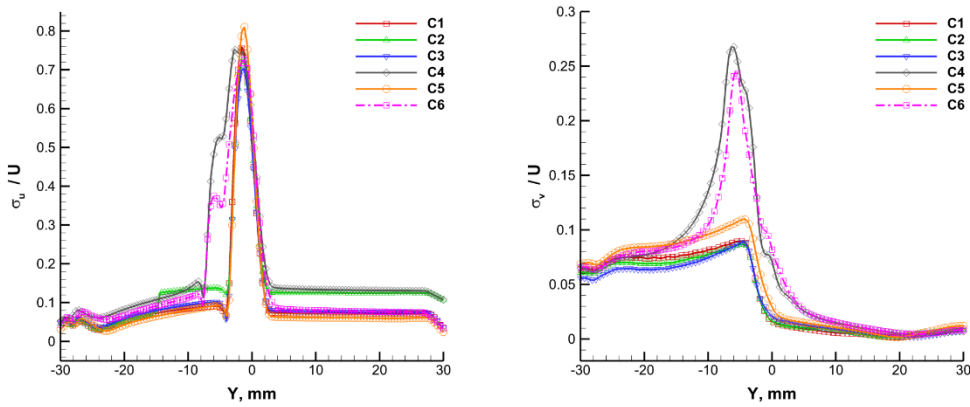


Figure 12: Shear mixing layer turbulence intensity of downstream and tangential direction of C1-C6.

2) X=200mm

At 200mm of downstream direction, the rule is similar to that at 100mm. For the two groups of C1 and C2 without transition, the peak turbulence intensity of downstream direction is basically same. The peak of C3 and C5 two groups is similar to C1 and C2. And the peak value is about 1, which is 20% higher than that of 0.8 at 100mm. However, the peak value of C4 and C6 of 200mm is similar to that of 100mm. In other words, for shear mixing layer that has been transformed, the turbulence intensity of downstream direction is basically unchanged.

For turbulence intensity of tangential direction, the peak value of shear mixing layer without transition increases about 40%, and the peak value after transition increased about 100% significantly. The peak of each group without transition is less affected by the parameters of the Mc.

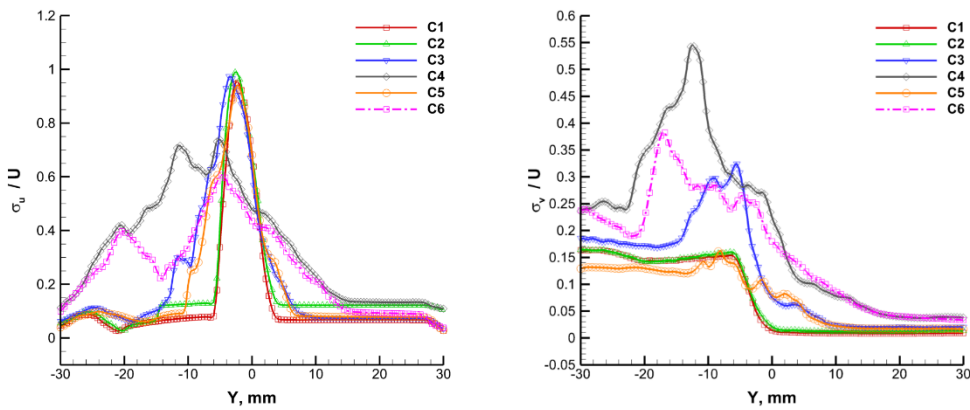


Figure 13: Shear mixing layer turbulence intensity of downstream and tangential direction of C1-C6.

As the Mc increases, the peak value of turbulence intensity of downstream direction remains the same basically, while turbulence intensity of tangential direction significantly decreases, and the rule is consistent with the research of shear mixing flow of weaker compressibility before, which shows that high temperature, high speed subsonic-supersonic shear mixing flow rule is similar to that of normal temperature, weaker compressibility shear mixing flow(including supersonic-supersonic and subsonic-supersonic shear mixing flow).

3.2.3 Reynolds stress

Reynolds stress is closely related to the flow structure. Zhou [21] pointed out that like $\bar{\rho} \widetilde{u''u''} / \rho_1 \Delta U^2$ appearing the bimodal structure in string direction is the embodiment of the hairpin vortex. In other literature, often use like $u'v' / \Delta U^2$ to nondimensionalize Reynolds stress $u'v'$, and usually the dimensionless method has good adaptability in smaller shear mixing flow velocity gradient. But in the large gradient shear mixing flow, velocity difference is huge, the $u'v'$ absolute value difference of two streams is very large, so using fixed value ΔU^2 to nondimensionalize has poorer adaptability. Therefore, in this paper, we use local U^2 to nondimensionalize the Reynolds stress.

Here, C1, C3 and C5 three groups are selected for analysis. The two groups of C1 and C3 have the same primary stream total temperature and the different Mc, which is used to compare the influence of Mc on the Reynolds stress of shear mixing flow. The two groups of C3 and C5 have the same Mc and the different primary stream static temperature, which is used to compare the influence of static temperature on the total Reynolds stress of the shear mixing flow in the same Mc.

At the center of the flow area, we make the XY cross section, and extract the $u'v' / U^2$ and $\langle u'v' \rangle / U^2$ in the cross section, which can obtain the Reynolds stress distribution of downstream direction of the shear mixing flow. Figure 14 and Figure 15 show the distribution of Reynolds stress of C1, C3 and C5 from top to bottom.

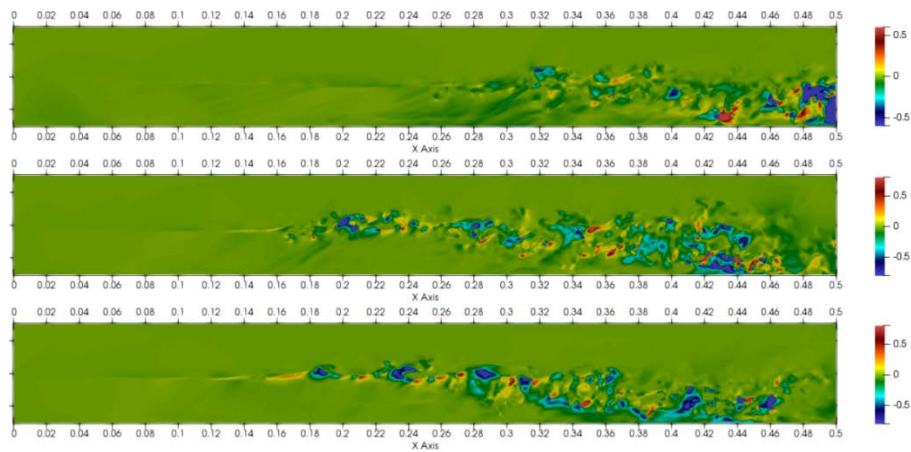


Figure 14: $u'v' / U^2$ distribution of downstream direction plane.

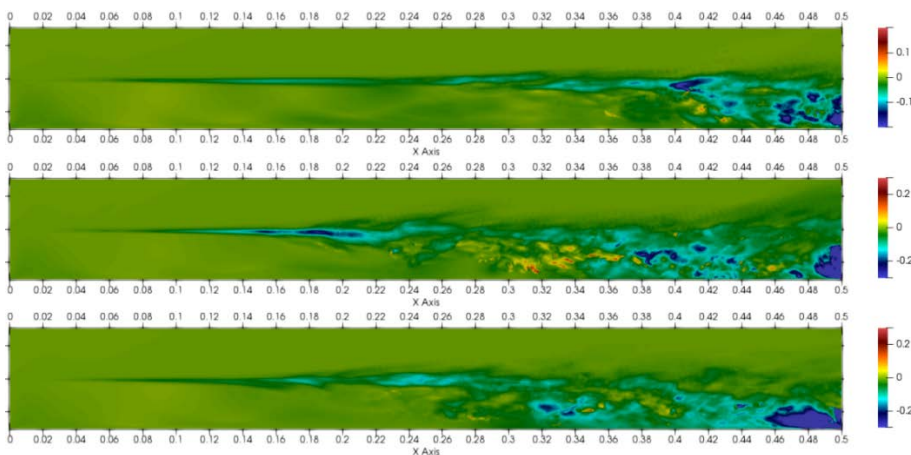


Figure 15: $\langle u'v' \rangle / U^2$ distribution of downstream direction plane.

Figure 14 is the instantaneous distribution of $u'v'/U^2$ of downstream direction plane. In the three groups of flows, the dimensionless Reynolds stress extreme values of C3 and C5 are close, but larger than that of C1, and the distribution of C3 and C5 is more intense.

In both groups of C3 and C5 ($Mc = 1.19$), Reynolds stress distribution pattern is extremum of positive and negative appearing alternately between $X = 0.10-0.22$ m, corresponds to the Λ vortex structure in flow (the cross section shape of spanwise and K-H instability caused coherent structure similar). In the case of C1 ($Mc = 1.67$), there is no obvious coherent structure always. Compared with previous research of shear flow, with the improvement of compressibility and Λ vortex structure in flow became clear, three-dimensional characteristics gradually increase.

When the two groups of C3 and C5, $X > 0.25$, reached the stage of full development, they showed the rule of positive extremum and negative extremum distribution, but they also contained certain fluctuations in each distribution. As the shear flow continues to develop downstream, the distribution of the Reynolds stress order is no longer obvious. However, it is very difficult for C1 group to observe such a regular phenomenon, indicating that the flow structure differs greatly from that $Mc=1$ after the further increase of the Mc .

Figure 15 is a distribution contour of $\langle u'v' \rangle / U^2$ in the direction of flow plane. The three groups of flows are similar in the laminar flow region, but the laminar state of C1 is much longer than that of C3 and C5. The Reynolds stress distribution of C3 and C5 is approximate. The Reynolds stress negative extremum of three groups is distributed in the subsonic region of the development area, and the supersonic region has no large flow structure. The rule and is very difference from shear mixing flow of lower compressibility. For shear mixing flow of $Mc > 1$, high compressibility prevented the formation of large scale coherent structures in supersonic region, only to form large scale coherent structures in low compressibility subsonic region. It also provides a certain enlightenment of shear mixing flow enhancement, namely for high compressibility shear mixing flow, pressing disturbance on supersonic region is not easy to cause the instability of flow, pressing disturbance on subsonic region should be considered. In addition, in the calculation of this paper, the height of the flow region is narrow, and the development of shear mixing flow structure is also affected.

Do XZ section in the center of the flow region, and extract $u'v'/U^2$ and $\langle u'v' \rangle / U^2$ at the section, we can obtain the spanwise distribution of Reynolds stress in the center of shear mixing flow. Figure 16 and Figure 17 show the distribution of the Reynolds stress in the three groups of C1, C3 and C5 from top to bottom.

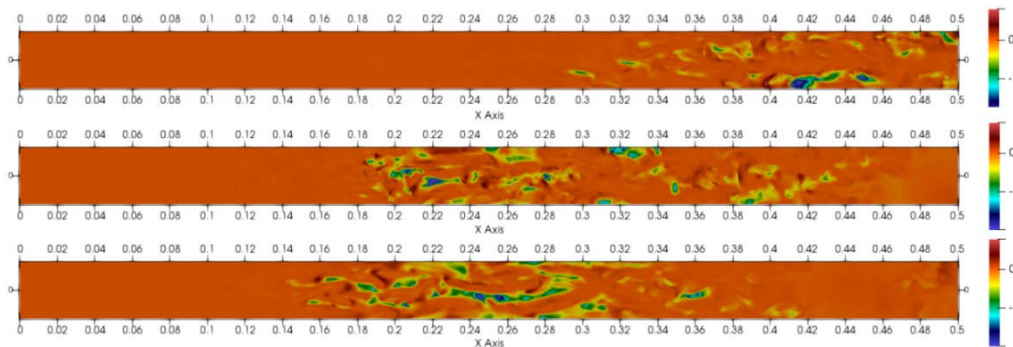


Figure 16: $u'v'/U^2$ distribution of spanwise direction plane.

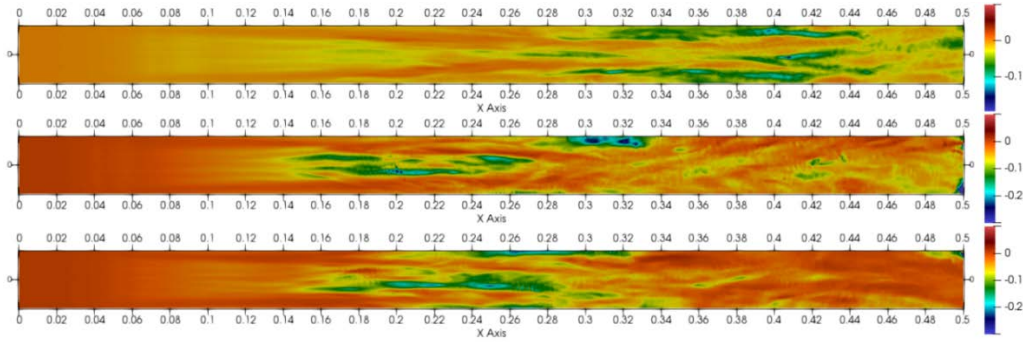


Figure 17: $\langle u'v' \rangle / U^2$ distribution of spanwise direction plane.

Figure 16 shows the instantaneous spanwise distribution of $u'v'/U^2$. On the whole, $u'v'/U^2$ distribution of C1 clearly focuses on the back of the flow region, starting from the $X = 290$ mm, weaker distribution appears along the flow, and the strength is very weaker than C3 and C5 groups. The rule is same with the rule of distribution in the direction of flow. C3 and C5 two groups appear zonal Reynolds stress distribution of $u'v'/U^2$ at $X = 180$ mm and $X = 140$ mm respectively. Compared with C1, the two groups are more close to.

The transient distribution of turbulent flow has a certain randomness. Therefore, the Reynolds stress spanwise distribution of the subsonic-supersonic shear mixing layer is investigated by means of averaging Reynolds stress distribution. Figure 17 shows the spanwise distribution contours of $\langle u'v' \rangle / U^2$. It can be obviously found that Reynolds stress distribution shows up band structure, and presents the positive extremum and negative extremum alternative distribution rule, there are certain rule of alternating in flow direction, but not obvious. The two groups of C3 and C5 show a clear band structure at $X=140$ mm, and the C1 group begins to appear at $X=260$ mm, significantly later than the C3 and C5 groups. C3 and C5 two groups have same Mc and different static temperature (1000 K and 473K). The two groups have similar flow structure, which explains static temperature have less effect on the shear mixing flow.

For Reynolds stress analysis of large gradient shear mixing flow of C1 and C3 two groups, can be found the dimensionless Reynolds stress (ratio) decreases with the increases of the Mc . The rule of flow structure variation is similar with the shear mixing flow of weaker compressibility, but Λ vortex structure becomes unclear, and three-dimensional characteristics gradually increase.

3.2.3 Vortex structure characteristics

Studied the evolution of coherent structures, can help us better understanding the development process of transition from layer to turbulent state and the turbulent flow mechanism, thus providing the reference for the research of the control of turbulence, turbulence model and LES. The shear mixing layer in the high compressibility condition is difficult to form the large scale coherent structure, but is small vortex highly fragmented. It is difficult to use the experiment to observe the vortex structure of the shear mixing layer. Because of LES can relatively fine reflect the characteristics of the vortex structure of shear mixing layer, and can easily get velocity field and density field, so the method is used to analyze the structural characteristics of the shear mixing layer. Researching coherent structure, coherent structure identification problem must be considered. Coherent structure of turbulent flow field more appear in the form of vortex structure, therefore coherent structure recognition method is based on identification of a vortex.

"Vortex" is a very common concept, but its definition is very vague, and it is difficult to give strict mathematical definition. Different from the concept of vortex, vorticity is defined as the curl of

velocity. However, the concept of vortex and vorticity in actual flow is different.

At present, the commonly used method of vortex identification is the criterion of pressure equivalent surface, the second invariant Q criterion of velocity gradient tensor, λ_2 criterion of Jeong et al. and Blackburn et al.

Q criterion:

$$Q = \frac{1}{2}(|\Omega|^2 + |S|^2)$$

Where:

$$S_{ij} = \frac{1}{2}(u_{i,j} + u_{j,i})$$

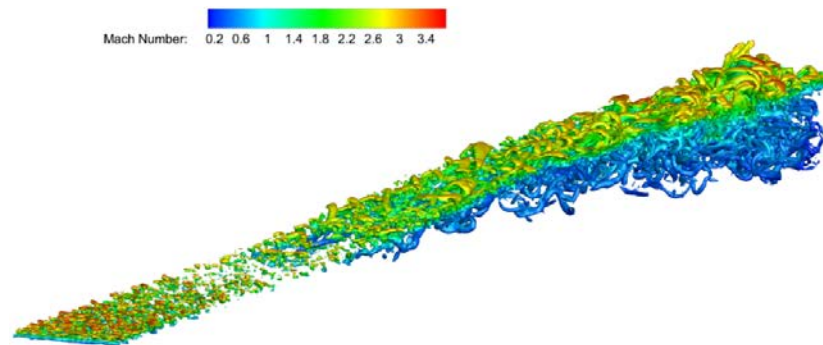
$$\Omega_{ij} = \frac{1}{2}(u_{i,j} - u_{j,i})$$

λ_2 criterion:

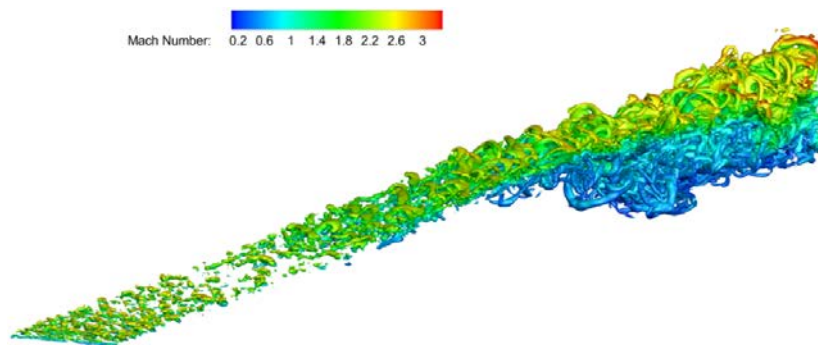
$$\text{Matrix } -S_{ik}S_{kj} - \Omega_{ik}\Omega_{kj}$$

Where: λ_1 , λ_2 and λ_3 is the eigenvalue of the matrix is taken, and $\lambda_1 < \lambda_2 < \lambda_3$, λ_2 is taken.

Here, the Q criterion is selected as the display method of the vortex structure. When the Mc increases, the vortex structure in the flow decreases, especially on the side of the high speed region, which can be clearly detected by comparing figure 17. This is because Mach number of primary stream increases, leading to enhancement of compressibility, flow is difficult to roll up large scale vortex structure after a disturbance, which through the vortex structure display method such as Q criterion, the part of primary stream is more "flat".



(a) Q criterion isosurface contour of C1 (staining by Ma).



(b) Q criterion isosurface contour of C2 (staining by Ma).

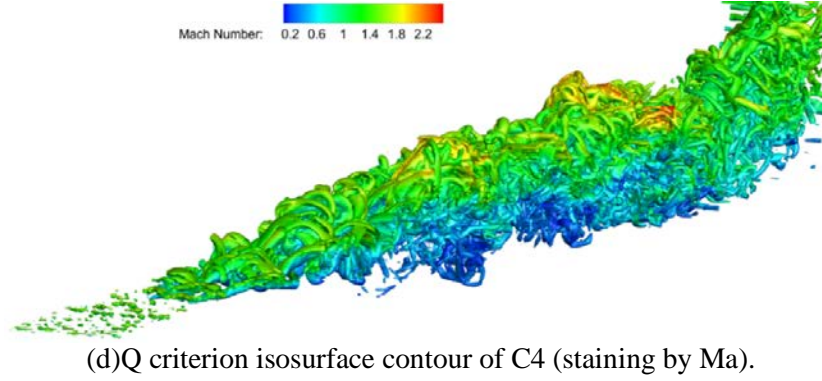
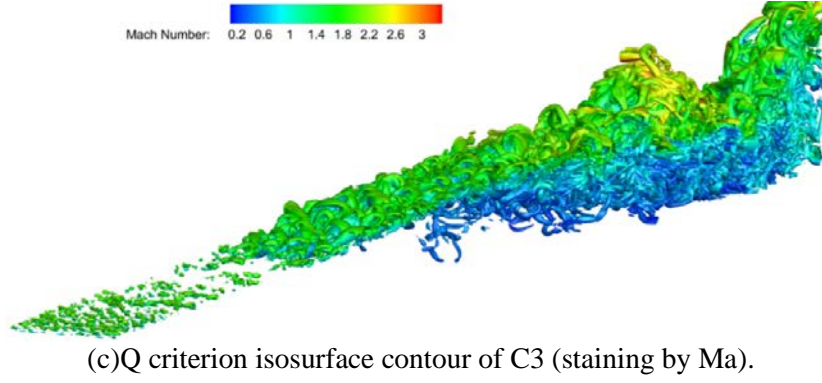


Figure 18: Q criterion isosurface contours of C1-C4 (staining by Ma).

In the shear flow of high compressibility, three-dimensional flow proportion is very big, difficult to observe Λ vortex structure. In the short distance after transition, the three-dimensional flow characteristics are strong, the vortex structure is wavy and chaotic, and it is difficult to observe the small scale coherent structure.

3.3 Shear mixing layer thickness growth rate characterization

$\delta(x)$ is defined as the shear mixing layer thickness at the position of x in downstream direction, and $\delta'(x)$ is the growth rate of shear mixing layer thickness. For linear shear mixing layer thickness growth rate, $\delta'(x)$ can be expressed as:

$$\delta'(x) \approx \frac{\delta(x) - \delta(x_0)}{x - x_0}$$

When $x \gg x_0$, $\delta'(x)$ can be expressed as the linear growth rate of shear mixing layer thickness.

At the same density ratio and velocity ratio, the growth rate of the shear mixing layer thickness of Mc to 0 is the growth rate of incompressible shear mixing layer thickness. The time growth model of Brown [22] and the spatial growth model of Dimotakis [23] all give the expression formula for the growth rate of incompressible shear mixing layer thickness:

$$\delta'_0 \approx C_\delta \frac{(1-r)(1+s^{1/2})}{2(1+s^{1/2}r)} \left\{ 1 - \frac{(1-s^{1/2})(1+s^{1/2})}{1+2.9(1+r)/(1-r)} \right\}$$

Where, $0.25 \leq C_\delta \leq 0.45$, and the specific value is related to the downstream conditions and other parameters in the experiment.

Compared with the experimental data, Brown [24] found that the condition of $1/7 \leq s \leq 7$ and $0 \leq r \leq \sqrt{1/7}$ has a better fit.

Bring related parameters of the 6 groups into the formula, to get each corresponding incompressible shear mixing layer thickness growth rate δ'_0 and shear mixing layer and the thickness growth rate δ' . Shown in table 2.

Table 2: Growth rate of shear mixing layer thickness in each group.

	C1	C2	C3	C4	C5	C6
δ'_0	0.334	0.382	0.438	0.491	0.256	0.337
δ'	0.0280	0.0360	0.0655	0.0858	0.0671	0.0799

Using the incompressible shear mixing layer thickness growth rate δ'_0 to nondimensionalize the compressible shear mixing layer thickness growth rate δ' , can get the thickness growth rate δ'/δ'_0 of each group, and gives the corresponding Mc and Π_c , shown in table 3.

Table 3: Mc , Π_c and thickness growth rate correspondingly.

	C1	C2	C3	C4	C5	C6
δ'	0.0280	0.0360	0.0655	0.0858	0.0671	0.0799
δ'/δ'_0	0.0838	0.0942	0.150	0.175	0.262	0.237
Mc	1.67	1.44	1.19	0.91	1.19	0.87
Π_c	2.61	2.42	2.14	1.76	1.70	1.46

C1 - C4 and C6 three groups, Ma , in turn, is reduced, while the thickness growth rate δ'/δ'_0 , in turn, increases, conforming to the rule of experiment research. The Mc of C5 is the same as that of C3, but the thickness growth rate is 1.75 times of C3; and the Mc of C5 is larger than that of C4 and C6, but the thickness growth rate is greater than that of these two groups. This indicates that the Mc does not accurately represent the growth rate of shear mixing layer thickness.

Through a large number of experimental studies previously, can summary the fitting formula with the characterization of Π_c [14]:

$$\frac{\delta'}{\delta'_0}(\Pi_c) = (1 + \alpha(\Pi_c)^2)^{-\beta}$$

Where, $\alpha \approx 4$, $\beta \approx 0.5$.

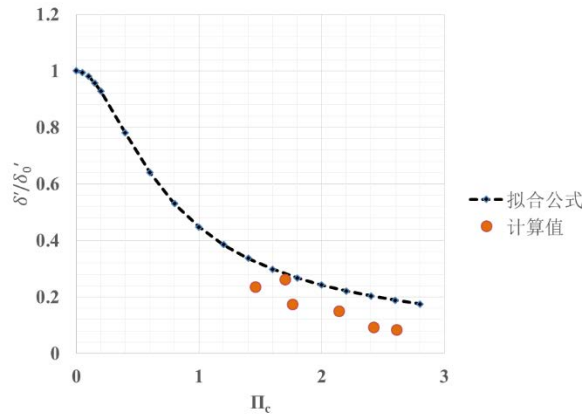


Figure 19: Fitting formula and calculation value.

Figure 19 shows the fitting formula and calculated values, the dotted line for the fitting formula, the dot for numerical calculation under different Π_c . Figure 19 shows that the calculated values is

significantly lower than that given by the fitting formula, but the distribution rule is similar to that of the fitting formula. This is mainly because the disturbance in the numerical simulation is relatively monotonous, while in the experiment, there are many disturbances, which have a strengthening effect on the shear mixing layer. Moreover, most disturbances are difficult to be modeled and can't be represented in numerical simulation.

When Π_c as characteristic parameter, $C1 - C4$ and $C6$, Π_c in order to reduce, while the thickness growth rate, in turn, increases, conforming to the rule of experiment research, and $C5$ still don't meet this rule, but the characterization effect is better than the Mc .

4 Conclusions

Aimed at high temperature, high speed large gradient shear mixing flow, this paper carried out LES of high order accuracy, obtained the flow characteristics of subsonic-supersonic shear mixing flow and growth rate of shear mixing layer thickness under the condition of different flow parameters, the results show that the development of subsonic-supersonic shear mixing flow with the following rules:

- With the increase of compressibility, the growth rate of shear mixing layer thickness decreases significantly. When the convective Mach number continues to increase to 1.44, the amplitude of thickness growth rate decrease decreases. The growth rate of $Mc=1.67$ is about 32.6% of $Mc=0.91$, while the growth rate of $Mc=1.44$ is 41.9% of $Mc=0.91$, decreased 22.2%.
- If the growth rate of the incompressible shear layer is defined as the dimensionless shear growth rate, the growth rate of $Mc=1.67$ is about 47.9% of $Mc=0.91$, while the growth rate of $Mc=1.44$ is 53.8% of $Mc=0.91$, decreased 11%. Compared with the absolute growth rate, the increase in growth rate is smaller when Mc increases from 1.44 to 1.67.
- In the case of the same convective Mach number, the primary flow static temperature has little influence on the thickness growth rate of the shear mixed layer, and has less influence on the flow structure.
- The shear mixing flow with strong compressibility is similar to the shear flow with less compressibility in the shear layer growth rate, turbulence intensity and Reynolds stress. It shows that there is similarity between the two flow regimes.

Large gradient shear mixing flow characteristics of high temperature, high speed bring great difficulty to experiment and numerical calculation research. This paper studies have shown that strong compressibility shear mixing flow and weaker compressibility shear mixing flow have many similarities on the flow regimes, especially on the statistical quantities such as turbulence intensity and Reynolds stress. It shows that for high temperature, high speed and super shear flow research, can be appropriate to reduce the flow parameters such as temperature, speed, so as to greatly reduce the difficulty.

References

- [1] Bogdanoff D W. Compressibility effects in turbulent shear layers. *AIAA Journal*, 21.6: 926-927, 1983.
- [2] Papamosehou D, Roshko A. The compressible turbulent shear layer: an experimental study. *Journal of fluid Mechanics*, 197: 453-477, 1988.
- [3] Papamoschou, Dimitri. Structure of the compressible turbulent shear layer. *AIAA Journal*, 29.5: 680-681, 1991.
- [4] Bradshaw, Peter. Compressible turbulent shear layers. *Annual Review of Fluid Mechanics*, 9.1: 33-52, 1977.

- [5] Zhao, YuXin, et al. "The experimental study of interaction between shock wave and turbulence." *Chinese Science Bulletin*, 52.10 (2007): 1297-1301.
- [6] Samimy M, Elliott G S. Effects of compressibility on the characteristics of free shear layers [J]. *AIAA Journal*, 28.3: 439-445, 1990.
- [7] Dimotakis P E. Turbulent Free Shear Layer Mixing and Combustion [J]. *High-Speed Flight Propulsion Systems*, 265, 1991.
- [8] Chinzei N, Masuya G, Komuro T, et al. Spreading of two-stream supersonic turbulent mixing layers [J]. *The Physics of fluids*, 29.5: 1345-1347, 1986.
- [9] Clemens N T, Mungal M G. Large-scale structure and entrainment in the supersonic mixing layer[J]. *Journal of Fluid Mechanics*, 284: 171-216, 1995.
- [10]Wagner R D. Mean flow and turbulence measurements in a Mach 5 free shear layer [J]. 1973.
- [11]Naughton J W, CATTAFESTA III L N, SettleS G S. An experimental study of compressible turbulent mixing enhancement in swirling jets [J]. *Journal of Fluid Mechanics*, 330: 271-305, 1997.
- [12]Rossmann T, Mungal M G, Hanson R K. Evolution and growth of large scale structures in high compressibility mixing layers[C]. TSFP DIGITAL LIBRARY ONLINE. Begel House Inc., 2001.
- [13]Day M J. Structure and stability of compressible reacting mixing layers [M]. 1999.
- [14]Slessor, M. D., M. Zhuang, and P. E. Dimotakis. Turbulent shear-layer mixing: growth-rate compressibility scaling. *Journal of Fluid Mechanics*, 414: 35-45, 2000.
- [15]Olsen M G, Dutton J C. Planar velocity measurements in a weakly compressible mixing layer [M]. *AIAA Journal*, 1999.
- [16]Pantano, C., and S. Sarkar. A study of compressibility effects in the high-speed turbulent shear layer using direct simulation. *Journal of Fluid Mechanics*, 451: 329-371, 2002.
- [17]Sandham, N. D., and W. C. Reynolds. Three-dimensional simulations of large eddies in the compressible mixing layer. *Journal of Fluid Mechanics*, 22: 133-158, 1991.
- [18]Doris L, Teuauud C, Phnoc L T. LES of spatially developing 3D compressible mixing layer [J]. *Computational Fluid Mechanics*, 328: 567-573, 2000.
- [19]Pullin. Vortex-Based Model for Subgrid Flux of a Passive Scalar [J]. *Physics of Fluids*, 2(9): 2311-2319, 2000.
- [20]Steven G. Goebel, J. Craig Dutton. Experimental study of compressible turbulent mixing layers [J]. *AIAA Journal*, 29(4): 538-546, 1991.
- [21]Qiang Zhou, Feng He, M. Y. Shen. Direct numerical simulation of a spatially developing compressible plane mixing layer: flow structures and mean flow properties [J]. *Journal of Fluid Mechanics*, 711: 437-468, 2012.
- [22]Brown, G. L. The entrainment and large structure in turbulent mixing layers. *5th Australasian Conference on Hydraulics and Fluid Mechanics, Volume 1*. Vol. 1. 1975.
- [23]P.E Dimotakis. Two-dimensional shear-layer entrainment [J]. *AIAA Journal*, 24: 1791-1796, 1986.
- [24]Brown G L, Roshko A. On density effects and large structure in turbulent mixing layers [J]. *Journal of Fluid Mechanics*, 64.64: 775-816, 1974.